Results in Engineering 29 (2026) 108719

Contents lists available at ScienceDirect

Results in Engineering

journal homepage: www.sciencedirect.com/journal/results-in-engineering

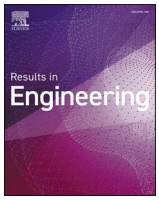

Molecular dynamics insights into allosteric and orthosteric co-targeting of *Mycobacterium tuberculosis* thymidylate kinase: A structure-based approach for bitopic ligand design

Amsaveni Sivaprakasam [a], Radha Mahendran [a,*], Umashankar Vetrivel [b,c], Luke Elizabeth Hanna [b,c]

[a] Department of Bioinformatics, School of Life Sciences, Vels Institute of Science, Technology and Advanced Studies (VISTAS), Pallavaram, Chennai, India
[b] Department of Virology and Biotechnology, ICMR-National Institute for Research in Tuberculosis, Chetpet, Chennai, India
[c] Academy of Scientific and Innovative Research (AcSIR), Ghaziabad-201002, Uttar Pradesh, India

ARTICLE INFO

Keywords:
Tuberculosis
Thymidylate kinase
Allosteric regulation
Molecular dynamics
Drug resistance

ABSTRACT

Allosteric regulation is a fundamental mechanism in enzyme function and drug design, enabling conformational changes upon ligand binding at sites distinct from the active site. In this study, we employed computational approaches to identify and characterize the allosteric site of *Mycobacterium tuberculosis* thymidylate kinase (TmpK), a crucial enzyme for bacterial nucleotide metabolism. The 3D crystal structure of TmpK (PDB ID: 1W2G) was analyzed for potential allosteric pocket residues using the PASSer server. Virtual screening and molecular docking studies revealed 4-Hydroxyestrone (4HY) as high-affinity binding moiety at both the orthosteric and allosteric sites, with docking scores of −11.5 kcal/mol and −7.1 kcal/mol, respectively. Molecular dynamics (MD) simulations also demonstrated that ligand binding at a single site to conserve structural stability, whereas simultaneous occupancy of both sites induced significant conformational perturbations, disrupting allosteric network. Pocket volume analysis also further indicated that ligand binding at one site dynamically modulated the cavity size of the other, driven by the mobility of the Ser150-Glu170 loop. Additionally, root mean square fluctuation (RMSF) analysis also highlighted increased flexibility in this region, reinforcing its role in allosteric regulation. These findings provide mechanistic insights into TmpK allostery and establish a computational framework for rational drug design. Furthermore, the study underscores the potential of allosteric inhibitors and bitopic ligands, which simultaneously target orthosteric and allosteric sites, as a promising strategy to combat multidrug-resistant tuberculosis, a critical challenge in global TB Elimination efforts.

1. Introduction

Mycobacterium tuberculosis (Mtb) is a highly infectious pathogen that causes tuberculosis (TB) in humans. The primary infection site is the lung, but it can also affect other organs through systemic dissemination that results in extrapulmonary form of TB. TB is currently the leading deadliest infectious killer surpassing COVID-19, as it led to death of around 1.25 million people out of 10.8 million people who contracted this disease [1]. TB cases are distributed across all regions, affecting men, women, and children worldwide, with vulnerable groups and certain countries bearing a disproportionate burden [2]. Multidrug-resistant TB (MDR-TB) continues to be a severe health threat, as only 2 in 5 people with MDR-TB have accessed treatment during 2023 [1,3]. The rise of multi-drug-resistant TB (MDR-TB) and extensively drug-resistant TB (XDR-TB) are the major concerns. MDR-TB does not respond to isoniazid and rifampicin, the two most powerful TB drugs in the first line Anti-TB treatment [4]. XDR-TB is resistant to even more drugs, making treatment highly complex and expensive. Current treatment for MDR/XDR-TB lasts for 9–24 months and has severe side effects [5].

Several drug targets have been explored and identified in *Mycobacterium tuberculosis*. Most of these targets focus on essential bacterial processes, such as cell wall synthesis, protein synthesis, and metabolism [6–8]. However, several mutations contributing to resistance to even some of the most potent antibiotics has been reported [9,10]. Notable mutations include those in the *katG* gene, which prevent the activation

* Corresponding author.
E-mail address: hodbioinfo@vistas.ac.in (R. Mahendran).

https://doi.org/10.1016/j.rineng.2025.108719
Received 1 June 2025; Received in revised form 29 October 2025; Accepted 11 December 2025
Available online 12 December 2025

of isoniazid. Mutations in the *embB* gene affect arabinosyl transferase, leading to alterations in arabinogalactan synthesis. Amino acid substitutions in the active site of the RNA polymerase β-subunit (*rpoB* gene) result in rifampicin resistance. Mutations in DNA gyrase (*gyrA* and *gyrB* genes) impact fluoroquinolone binding, contributing to resistance against this antibiotic class [11–13]. Hence, this poses a need for exploring newer alternative targets to address the issue of drug resistance.

Orthosteric sites are the primary binding regions on a protein where endogenous ligands or conventional drugs interact to exert their therapeutic effects. Most drugs are designed to directly target these sites, and either inhibit or activate the protein's function [14,15]. Drug resistance often arises from mutations at these sites, which reduce drug binding efficiency and render treatments ineffective [16,17]. Unlike orthosteric sites, allosteric sites are secondary binding sites on a protein that, when occupied by a ligand, induce conformational changes that affects the protein function. These sites are often less prone to mutations, making them promising target site for drug development. Allosteric modulators can work alongside orthosteric drugs to enhance efficacy, potentially lowering the required dosage and reducing side effects [18]. This concept has been majorly focused in the present as a means of combating drug resistance in *Mycobacterium tuberculosis.*

In pharmacological research, allosteric regulation has emerged as a significant model and is essential for influencing enzyme activity. In contrast to orthosteric inhibitors, which directly obstruct the catalytic site, allosteric ligands have the ability to regulate conformational dynamics, stabilize inactive states, or improve selective inhibition without directly vying with natural substrates [19,20]. This regulatory strategy is especially pertinent for nucleotide-metabolizing enzymes and kinases, as the conservation of catalytic sites frequently leads to off-target effects when conventional inhibitors are employed [21–23]. The precise prediction of enigmatic and druggable allosteric sites, which are extensively used in the discovery of antimicrobial drugs, has been made possible by recent advancements in computational structural biology [24–26].

Mycobacterium tuberculosis thymidylate kinase (TmpK) is a critical enzyme in the dTMP/dTTP biosynthetic pathway, responsible for the phosphorylation of dTMP to dTDP [27,28]. TmpK's potential as a therapeutic target has been underscored by genetic knockout studies, which have demonstrated its critical role in bacterial survival and reproduction [29]. Resistance, insufficient selectivity, and restricted efficacy have been obstacles encountered by conventional orthosteric inhibitors of TmpK [29,30]. In this context, the assessment of TmpK's allosteric regulation provides a viable alternative approach, which facilitates the identification of novel modes of action and the reduction of cross-resistance.

The identification of allosteric sites has been extensively investigated using computational techniques, such as cavity detection algorithms and network-based investigations of protein conformational dynamics [31–33]. The efficacy of employing in silico methods to predict and validate allosteric sites in bacterial enzymes has been demonstrated in numerous studies, thereby expediting early-stage drug development [34]. The discovery of druggable allosteric centers in kinases has broadened the potential of rational design approaches, allowing for the development of bitopic ligands that simultaneously interact with orthosteric and allosteric sites [35].

Mycobacterium tuberculosis thymidylate kinase (TmpK) is well documented as potential drug target for tuberculosis (TB) [36,37]. This enzyme is encoded by TmpK gene, and it plays a crucial role in maintaining nucleotide pools necessary for bacterial growth and survival. It enzymatically converts dTMP (thymidine monophosphate) into dTDP (thymidine diphosphate) utilizing ATP as a phosphate donor [38,39]. There is dearth of FDA-approved drugs specifically designed to target this Mtb enzyme. This enzyme is now actively being explored as a potential drug target, however, the development of specific inhibitors are still in the nascent stages, for instance, new *Mtb* TmpK inhibitors are majorly proposed based on computational and QSAR modelling studies [27,40]. In parallel, allosteric regulation of inosine 5′-monophosphate dehydrogenase, an essential enzyme of purine metabolism in *Mycobacterium* have shown possibilities for development of allosteric inhibitors with antibacterial potential [41] and recent research on the Mpro of SARS-CoV-2 has identified drugs and small fragments that bind to sites beyond the substrate-binding site, potentially influencing allosteric regulation [42,43]. These sorts of studies open up new avenues for exploring allosteric inhibitors as alternative strategy. Allosteric inhibitors are generally identified through *in silico* docking studies of small molecule drug libraries etc., [44,45]. Targeting TmpK offers a novel and promising approach for the development of anti-tubercular drugs, especially in the fight against multidrug-resistant (MDR) and extensively drug-resistant (XDR) tuberculosis. With ongoing research, TmpK inhibitors hold the potential to become an integral part of next-generation TB treatments [46,47]. Inhibitors of TmpK are being explored as potential antimycobacterial drug to combat against tuberculosis, particularly in the wake of increasing drug resistance [48,49]. The bacterial thymidylate kinase (TmpK) structure and mechanism differ from those in humans, presenting an opportunity for selective inhibition with minimal toxicity to human cells [50]. Hence, this study aims to predict the allosteric site in the TmpK gene of *Mycobacterium tuberculosis* (Mtb), to investigate the intramolecular network between the active and allosteric sites, and to demonstrate the allosteric site's influence on ligand binding at the active site cavity.

TmpK is an unexplored yet highly compelling target for the structure-based design of bitopic inhibitors, given the imperative need for innovative treatments for multidrug-resistant tuberculosis (MDR-TB). By incorporating molecular docking, allosteric site prediction, and molecular dynamics simulations, this research enhances comprehension of TmpK regulation. The objectives of our research are to elucidate the molecular mechanisms of TmpK allostery, establish computational standards for inhibitor design, and encourage the expanded development of allosteric and bitopic ligand strategies in the field of anti-TB drug discovery.

Fig. 1

2. Materials and methods

2.1. Protein structure data retrieval and allosteric site prediction

The crystal structure of *Mycobacterium tuberculosis* thymidylate kinase in complex with Deoxythymidine (dT), was retrieved from the Protein Data Bank (PDB) using the accession code [PDB ID: 1W2G, 2.1 Å, Chain A and Chain B, (214 residues per chain)]. Structurally, this monomeric enzyme adopts a α/β nucleotide kinase fold, characterized by a central five-stranded parallel β-sheet flanked by α-helices on both sides. The active site is located in a cleft between the CORE domain, which contains the ATP-binding motif, and the LID domain, which undergoes conformational changes upon ligand binding. Further, structure was geometry optimized and utilized for allosteric site prediction. PASSer (Protein Allosteric Sites Server), a web-based application was used for allosteric site prediction and visualization. It predicts on the basis of three trained machine learning models: (1) ensemble learning through extreme gradient boosting and graph convolutional neural network; (2) automated machine learning through AutoGluon framework; and (3) learning to rank through lightgbm. In this study, the refined structure of M.tb TmpK (PDB ID: 1W2G, 2.1 Å, Chain A and Chain B, excluding Deoxythymidine (dT)) in PDB format was uploaded into the server along with chain ID (Chain A, as the protein is a monomer) specifying the Ensemble learning type of trained model to predict the allosteric pockets [51].

2.2. Virtual screening using MTiOpenScreen

Recent evidence shows that estrogen and its receptors play key roles in antibacterial defense mechanisms, influencing both immune cell

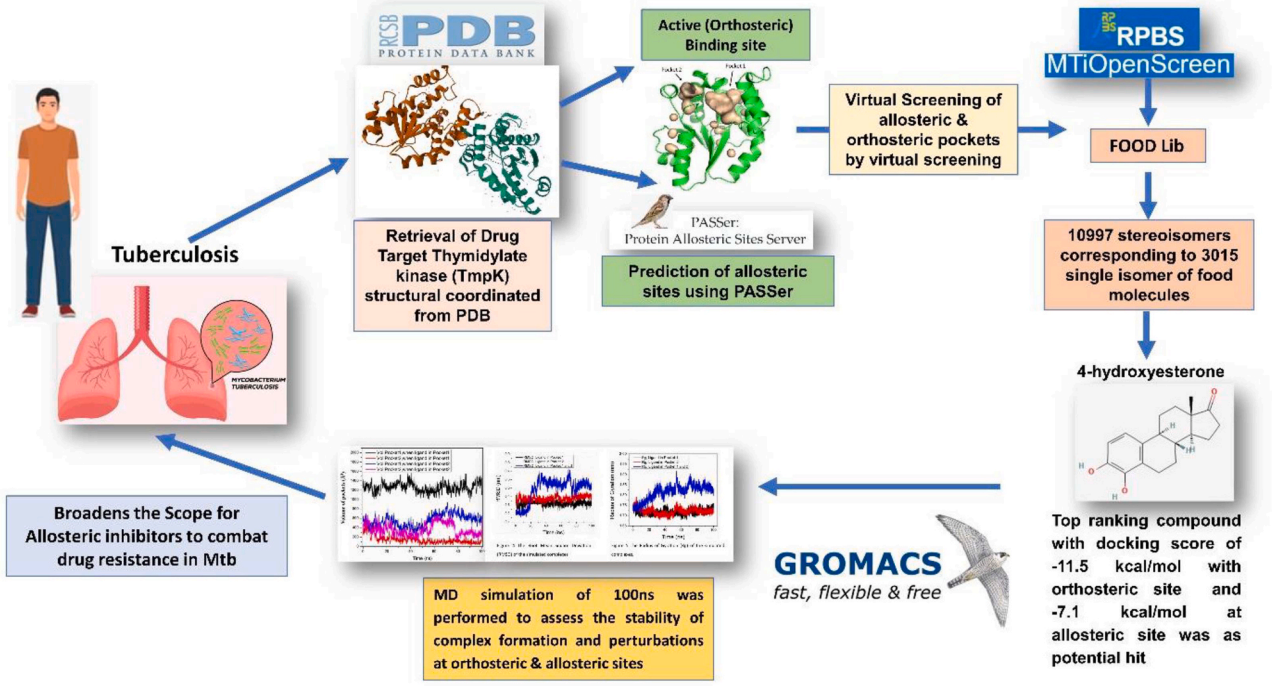

Fig. 1. *Insilico* workflow implemented in this study.

function and bacterial clearance [52]. In the context of tuberculosis, host-directed therapies (HDTs) that modulate metabolism and immunity are gaining traction [53–54]. It is now well established that *Mycobacterium tuberculosis* is heavily dependent on host lipid metabolism for its intracellular survival, and that perturbation of fatty acid import or catabolism in macrophages markedly impairs bacterial growth [55]. Moreover, dietary and microbial modulation of estrogen metabolites has been shown to affect the circulating metabolome and microbial composition [56]. Taken together, these findings suggest that food-derived estrogen metabolites, which already act on host metabolism/immunity and are subject to dietary/absorptive pathways, are credible chemical scaffolds for further optimisation as TB-therapeutic leads.

MTiOpenScreen performs automated virtual screening using AutoDock Vina [57] which is a online tool for structure-based virtual screening. MTiOpenScreen enables virtual screening using five chemical libraries including predefined diverse compound collection (Diverse-lib) focused chemical compound collection (iPPI-lib) to target protein-protein interactions (PPI), purchasable approved drugs (Drugs-lib), food constituent compound collection (FOOD-lib) and a natural product compound collection (NP-lib). Given the critical role of TmpK in the thymidine biosynthesis pathway of *M. tuberculosis*, targeting this enzyme with food-derived, metabolically accessible compounds offers a strategic advantage in the search for novel antimycobacterial agents. Additionally, leveraging food-derived compounds increases the potential for repurposing dietary bioactives as therapeutic leads, reducing the risk of toxicity and enhancing translational applicability. Hence, FOOD-lib was selected for identifying promising, safe, and pharmacologically relevant inhibitors of *M. tuberculosis* TmpK. FOOD-lib, encompassing 10,997 stereoisomers corresponding to 3015 single-isomer food constituents, was subjected to virtual screening [58] to identify both orthosteric and allosteric inhibitors, and to find a common compound with the ability to target both sites with greater binding affinity.

The 3D crystal structure of the protein TmpK enzyme was retrieved from the RCSB Protein Data Bank (PDB) with the ID: (PDB Id: 1W2G) [59] and structure of 4HY (ligand) was obtained from PubChem (https://pubchem.ncbi.nlm.nih.gov/compound/9971251). Both the structures were refined and geometry optimized prior to docking.

2.3. Toxicity prediction

ProTox3.0 is a web server designed to predict the oral toxicity of small molecules in rodents. It estimates theoretical LD_{50} values and toxicity classes based on the structural similarity of chemical compounds to known toxic substances [60]. This tool was used predict the toxicity profile of the selected compounds.

2.4. Preparation of receptor and ligand for molecular dynamic simulations

2.4.1. Receptor structure preparation

Missing amino acid regions of the TmpK structure (PDB Id: 1W2G, 2.1 Å Chain A) from residues150–161, residues 209–214 were modelled and energy minimized (2000 steps conjugate gradient and 1000 steps steepest descent) using Swiss-PDBViewer program, with GROMOS96 set as force field [61]. The Chain A of refined crystal structure of TmpK (PDB ID: 1W2G) was analyzed to identify different allosteric ligand binding pockets.

2.4.2. Molecular docking

The structure of the small molecule which featured as the bitopic ligand targeting both orthosteric and allosteric site during initial virtual screening against Food-lib was built and optimized with the 6–31G/B3LYP method using Orca 5.1 program. The optimized ligand molecule was docked to the refined TmpK enzyme(both orthosteric and allosteric sites) structure using Autodock vina v 1.1.2 [62]. The essential PDBQT files for protein was generated using MGL Tools v.1.5.4 [62] by assigning Kollman united charges. Similarly, the PDBQT files for ligand molecule was generated by assigning Gasteiger charges. The grid box was centered on the two pockets (Pocket 1 and Pocket 2). All other docking parameters were assigned to their default optimal values. The best docked pose was selected based on binding energy and was utilized for further analysis. The binding conformation and hydrogen bonded interactions of the ligand molecule within the active site cavity was visualized and tabulated.

2.4.3. Molecular dynamics simulation

Molecular dynamics (MD) simulation for the protein-ligand complexes was performed using GROMACS v2022.2 with CHARMM36, set as force field [63,64]. The ligand structure for 4-HY was constructed with the CHARMM General Force Field (CGenFF), and the preliminary penalty scores were assessed [65]. The charge penalty was 49.7, categorizing it within the moderate range as per CGenFF rules, suggesting that the allocated partial charges are somewhat dependable. These standards stipulate that penalties ranging from 10 to 50 denote moderate confidence. Consequently, the ligand parameters are considered suitable for molecular dynamics research in conjunction with CHARMM36 for the protein. The complex system was solvated with TIP3P water model, and neutralized with appropriate number of Na^+ and Cl^- ions. Energy minimization was performed by steepest descent method with 50,000 steps for all systems with a tolerance of 1000 kJ mol-1 nm-1. Equilibration steps were carried out for 1 ns for each system with a constant number of particles, volume, and temperature (NVT; with modified Berendsen thermostat with velocity rescaling at 310 K and a 0.1 ps time step) and a constant number of particles, pressure, and temperature (NPT; Parrinello−Rahman pressure coupling at 1 bar with a compressibility of 4.5×10^{-5} bar^{-1} and a 2 ps time constant). Nosé−Hoover thermostat was used in NPT equilibration and final production run to produce an optimal kinetic ensemble. Bond lengths were constrained using the Linear Constraint Solver (LINCS) algorithm [66–67]. To confirm that the deployment of the LINCS technique for restricting bond lengths did not generate artifacts during the prolonged 100 ns simulation period, the trajectories were meticulously checked for stability. No breaches of constraints, unexpected deviations in bond lengths, or high-energy frames were observed during the production run. The overall energy, temperature, and pressure profiles remained consistently equilibrated without sudden spikes, signifying the lack of instabilities or numerical aberrations. For long-range interactions, the particle-mesh Ewald (PME) [68,69] method was used with a 1.2 nm cutoff and a Fourier spacing of 0.16 nm. Two step-simulation strategy was adopted, where in the first phase 10 ns MD-simulation was carried out with restrained backbone and subsequently 100 ns production run was performed. To ensure the reliability of our results we repeated the simulations twice for each system, and trajectories were sampled at every 10 ps for data analysis [70–71]. During the molecular dynamics simulations, periodic boundary conditions (PBC) were carefully addressed to ensure accurate analysis of pocket volumes and inter-domain distances. Prior to all structural analyses, the trajectory frames were re-centered on the protein and imaged to remove any artifacts caused by molecules crossing the simulation box boundaries. Specifically, gmx trjconv (GROMACS) was used to re-center the protein and apply the "-pbc mol -center" option, ensuring that all residues and ligands remained within a single, continuous image of the protein. This procedure guarantees that the cavity volume calculations (pocket 1 and pocket 2) reflect the true spatial dimensions of the binding sites over time, without distortions from periodic wrapping.

3. Results

3.1. Allosteric site prediction and orthosteric site of Mtb TmpK protein

TmpK structure was probed to identify different allosteric ligand binding pockets using PASSer. These allosteric sites may have the ability to modulate the active site cavity, thereby modulating catalysis. An additional binding site spanning amino acid residues Arg149, Gly10, Val8, Ala11, Gly12, Lys13, Arg14, Thr15 comprising volume of ~262.38 $Å^3$ other than the catalytic site residues: Tyr165, Tyr103, Asn100, Ser99, Phe70, Pro37, Arg95, Phe36, Pro37, Tyr39, and Arg74 with a volume of ~1000 $Å^3$ (Fig. 2 and 3) was predicted by PASSer. Moreover, active catalytic site predicted by the PASSer was also found to corroborate with the documented catalytic sites reported earlier [22–24], thereby ensures the predictive accuracy of the method implemented.

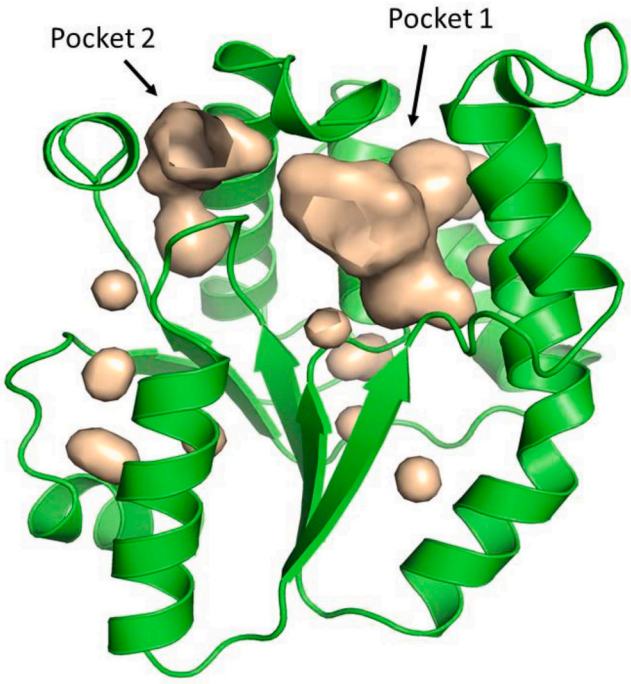

Fig. 2. Identification of an allosteric pocket (pocket 2) from 1W2G crystal structure. The active site cavity is marked pocket 1.

The allosteric site of the protein Mtb TmpK, as predicted by PASSer, (Pocket.2) was found to be highly plausible with a significant probability score of 43.02 %, spanning the key residue stretches: 8–11, 138–153 and 162–180.

The allosteric site of Thymidylate Kinase (TMK) was initially predicted using the PASSer server. To validate this prediction, this study employed the STINGAllo web server, which identifies allosteric site-forming residues based on internal protein nanoenvironment descriptors [72]. STINGAllo identified residues Gly10, Ala11, Gly12, Lys13, Arg14, and Thr15 as forming the allosteric site, which overlap with the residues predicted by PASSer, confirming the consistency between the two methods. This cross-validation supports the reliability of the predicted allosteric pocket and strengthens the rationale for targeting it in subsequent docking and MD simulation studies.

3.2. Toxicity prediction by ProTox3.0

As per ProTox prediction, the LD_{50} of 4HY is 5000mg/Kg and categorized as category 5 substance (i.e., Class V: may be harmful if swallowed ($2000 < LD_{50} \leq 5000$). The toxicity values have been compared with standard anti-TB drugs Rifampicin (RIF) and Isoniazid (INH), whose LD_{50} has been predicted as 500mg kg^{-1} and 133mg kg^{-1}, respectively. No significant hepatotoxicity, neurotoxicity, nephrotoxicity, carcinogenicity, mutagenicity, or general cytotoxicity is noted for 4HY when compared to the toxicity levels of RIF and INH with hepatic, nephron and neurotoxicity (Complete details are provided as supplementary Table 1).

In addition to assessing toxicity (LD50), we performed a comprehensive ADMET and drug-likeness evaluation for 4-Hydroxyestrone (4HY) using ProTox3.0. The analysis included predictions of organ toxicity (hepatotoxicity, neurotoxicity, nephrotoxicity, respiratory toxicity, cardiotoxicity), toxicity endpoints (carcinogenicity, immunotoxicity, mutagenicity, cytotoxicity, BBB permeability, ecotoxicity, clinical and nutritional toxicity), Tox21 nuclear receptor signaling pathways (AhR, AR, ER, PPAR-γ, etc.), Tox21 stress response pathways (NRF2/ARE, HSE, MMP, p53, ATAD5), molecular initiating events (THRα/β, TTR, RYR, GABAR, NMDAR, AMPAR, KAR, AChE, CAR, PXR,

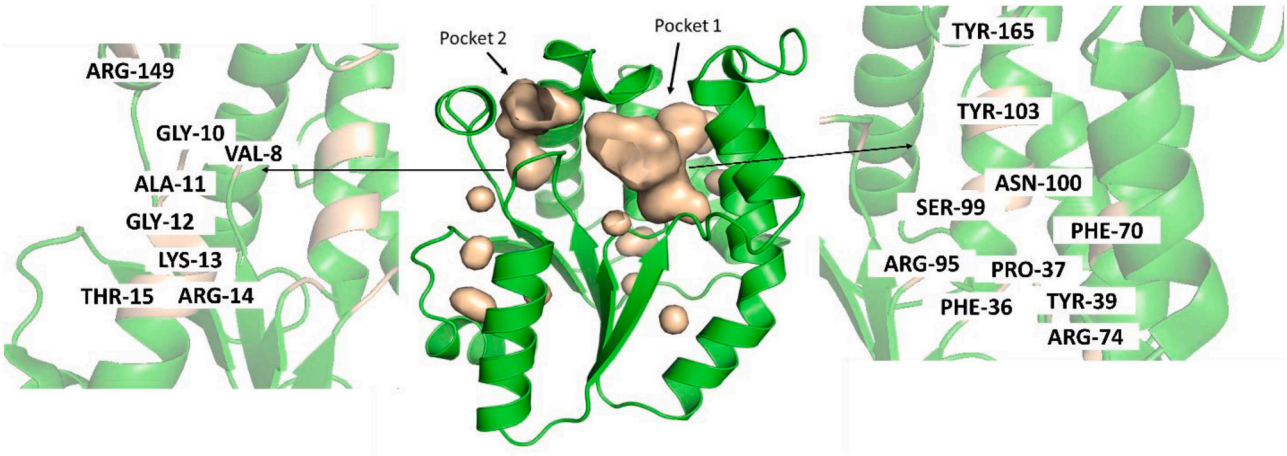

Fig. 3. Details of aminoacid residues of active binding site (Pocket 1) and allosteric site (Pocket2).

NADHOX, VGSC, NIS), and metabolism-related predictions (CYP enzymes).

The results indicated that 4HY exhibited minimal organ and systemic toxicities compared to first-line anti-TB drugs (Rifampicin and Isoniazid), with a predicted LD50 of 5000 mg kg^{-1}, suggesting low acute toxicity. Some activity was noted for cardiotoxicity, respiratory toxicity, clinical toxicity, GABA receptor interaction, mitochondrial membrane potential (MMP), and certain nuclear receptors, but overall the profile is favorable. These results demonstrate that 4HY satisfies key drug-likeness and ADMET criteria, supporting its suitability as a lead compound for further pharmacological development.

3.3. Virtual screening

The virtual screening analysis with the "FOOD-lib" of MTiopenscreen resulted in the identification of, 4 hydroxyesterone (4HY) giving the highest docking score of − 11.5 kcal/mol at the active binding site of the enzyme and it is the topmost compound. Similarly, while assigning residues of pocket 2 as 'list of residues' during screening process 4HY had a docking score of −7.1 kcal/mol.

During the virtual screening and docking process, 4-Hydroxyestrone (4HY) was identified as the leading candidate, demonstrating significant binding affinity at both the orthosteric and allosteric sites of TmpK. The choice of 4HY was influenced by its dual high docking scores (−11.5 kcal/mol at the orthosteric site and −7.1 kcal/mol at the allosteric site), which ranked among the highest in the screening library. Furthermore, 4HY has been identified in various biological contexts, as an endogenous estrone metabolite, it has comparatively modest estrogenic activity relative to other hydroxylated estrogens, while demonstrating biological effects including neuroprotection and antioxidant properties [73,74]. These characteristics indicate that its biochemical foundation is rather acceptable and may enable derivatization to mitigate estrogenic off-target effects. While 4HY was the leading dual-site binder, other candidates were evaluated during the screening process. Multiple ligands exhibited robust binding in one pocket but demonstrated inadequate complementarity in the other, hence not meeting the dual-site binding threshold established in this study. Consequently, 4HY was not singular but was the sole compound in the collection to demonstrate high affinity at both locations according to the existing docking criteria. Incorporating these comparison statistics, specifically the leading candidates and their docking scores for both pockets, in a supplementary table would enhance transparency.

In order to provide context for the docking scores presented in this study, we conducted a comparison with TMK ligands that had been previously identified. The orthosteric region of TMK was bound by the most active molecule (M31) from the published dataset [27], resulting in a docking score of −8.90 kcal/mol. In this study, 4-Hydroxyestrone (4HY) exhibited a superior orthosteric binding score of −11.5 kcal/mol, indicating a higher affinity than the previously reported M31. The ligand docking score for the allosteric site was −7.1 kcal/mol, which suggests a substantial and potentially significant binding for allosteric regulation, despite being lower than the orthosteric binding score. This comparison with a recognized orthosteric ligand establishes a standard for evaluating the relative intensity of ligand interactions and validates the importance of this docking data for both active and allosteric locations. As this compound scored high docking score on both pockets, it was chosen further for MD simulations, to confirm communication between both the pockets.

3.4. Analysis of MD-simulation trajectories

Three different protein-drug complexes were modelled and analysed in this work. The ligand molecule, 4-Hydroxyestrone docked in pocket-1 of the enzyme (system 1), 4HY docked into pocket-2 (system 2) and two molecules of 4HY one each in pocket-1 and 2 (system 3). Dynamic Stability of these simulated complexes (system 1–3) were measured by root mean square deviation (RMSD) and Radius of gyration (Rg). Systems 1 and 2 were observed to be stable throughout the simulation trajectories with deviations ranging from 0.3 nm to 0.45 nm. However, system 3 was found to be unstable with the ligand molecules moving out

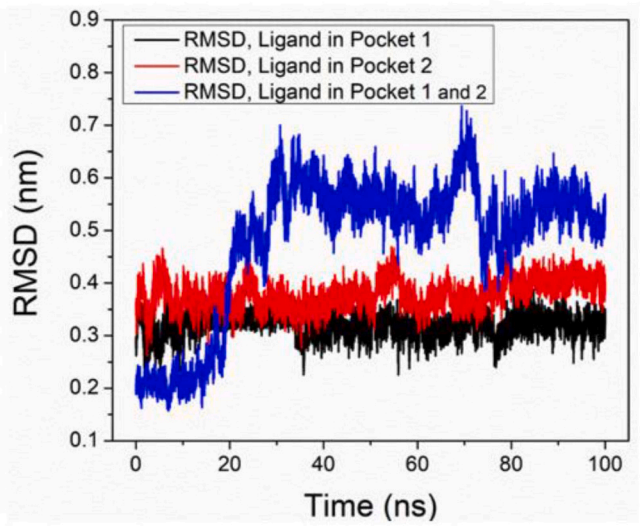

Fig. 4. The Root Mean Square Deviation (RMSD) of the simulated complexes.

of pocket 2 during simulations (Fig. 4).

The Radius of gyration (Rg) value indicates the compactness of the protein folds during simulation. Low values of Rg indicate high structural compactness and structural integrity, whereas high values of Rg indicate less structural compactness and less stability. Systems 1 and 2 showed Rg values ranging from 1.70 to 1.75 nm indicating high compactness while system 3 had Rg values ranging from 1.75 to 1.90 nm suggesting less compactness and stability (Fig. 5).

The instability noted in the dual-ligand system (system 3), where one ligand was displaced from pocket 2 during molecular dynamics simulations, offers essential insights into the difficulties of developing bitopic ligands. This finding does not necessarily contradict the core hypothesis of developing bitopic ligands but highlights the complexities involved in their design and the need for careful consideration of structural and dynamic factors. Bitopic ligands, which concurrently bind to orthosteric and allosteric sites, present the possibility of improved specificity and efficacy [75]. Nonetheless, their design must consider the structural and dynamic compatibility of both binding sites. The displacement of a ligand in system 3 indicates that the spatial and kinetic restrictions between the two pockets may not facilitate stable dual binding.

Prior research has documented analogous difficulties in the creation of bitopic ligands. Gaiser et al. (2024) shown that metastable binding sites (MBS) can function as allosteric binding sites (ABS) in ligand design, resulting in compounds with enhanced binding kinetics [76]. They also emphasized that the identification and validation of appropriate MBSs are essential for the success of such systems. Consequently, the instability shown in system 3 highlights the possible challenges in bitopic ligand creation, while also offering critical insights for enhancing design tactics. Future efforts should focus on optimizing linker design, ensuring favorable spatial and dynamic compatibility between binding sites, and employing advanced simulation techniques to predict and mitigate potential instabilities.

This study have not designed a single-molecule bitopic ligand with a covalent linker connecting the orthosteric and allosteric pharmacophores. The present findings, especially the instability noted in the dual-ligand system (system 3), offer critical insights for the future rational design of a genuine bitopic ligand, encompassing optimal linker length, flexibility, and chemical characteristics to guarantee stable concurrent engagement of both sites. Consequently, the current technique is confined to the co-administration of two identical ligands; nonetheless, it establishes a foundation for the future creation of a covalently connected bitopic molecule.

The volume of pockets 1 and 2 during MD simulations, the Ser150-Glu170 loop formed between the two helices (walls of pocket 2) are highly mobile and determines the cavity volume. When 4HY accommodates into pocket 1, the two pockets fuse making the cavity bigger and decreasing the volume of pocket 2. Two distinct pockets are observed when 4HY accommodates into pocket 2 by breaking the communication between pockets, as shown in Figs. 6 and 7.

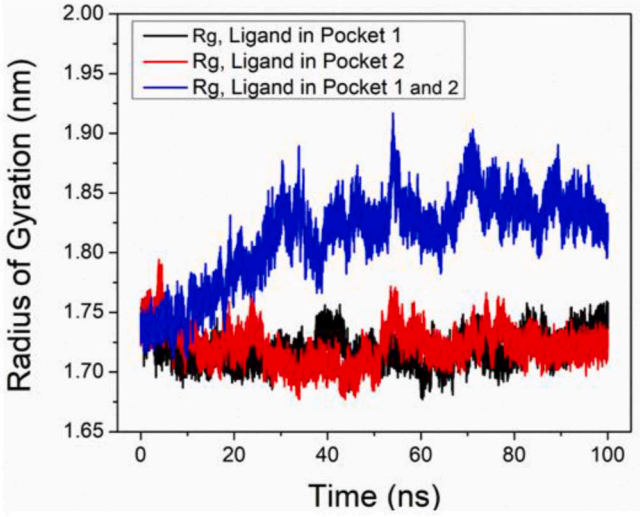

Fig. 5. The Radius of Gyration (Rg) of the simulated complexes.

Previous studies included a detailed Thymidylate Kinase (TMK) sequence and structure analysis, focusing on evolutionary conservation across species. Amino acid sequences of TMK from Human (CAA38528.1), Gorilla (XP_004033529.1), Guinea pig (XP_003474598.3), Mouse (NP_001099137.1), Zebrafish (NP_001032187.1), and Yeast (AAA35158.1) were aligned [77]. The analysis revealed that the Ser150-Glu170 loop is not part of the conserved residues across these species. This indicates that, although the loop contributes to pocket volume modulation in our simulations, it is not evolutionarily conserved and is unlikely to play a critical regulatory role in TMK function universally.

The analysis of volume of the simulated complexes showed that the volume of the pocket1 with 4HY was bound to be very high (~1200 to 1400 $Å^3$), whereas the volume of pocket 2 was found to have decreased (~400 to 100 $Å^3$)indicating that when the ligand (4-HY) occupies the active site cavity it expands and pushes the helices forming walls of the allosteric pocket (pocket 2) to inhibit ligand binding to pocket 2. Again, when 4HY was bound to pocket 2, the volume of this pocket ranged from ~400- 600 $Å^3$, with a corresponding decrease in the volume of pocket 1 (~500 to 700 $Å^3$) (Fig. 8).

Interaction analysis of 4-Hydroxyestrone (4HY) with Thymidylate Kinase (TMK) over the course of the 100 ns MD simulation revealed dynamic changes in binding contacts using LigPlot+ [78]. At the initial frame (0 ns), the ligand formed hydrogen bonds with Glu173 and hydrophobic contacts with Val8, Gly176, and Val193 within the active site. By the end of the simulation (100 ns), the ligand established hydrogen bonds with Val8 and Leu139, while hydrophobic interactions were observed with Ala11, Gly7, Val141, and Gly176.

These results indicate that while the ligand remains bound within the active site throughout the simulation, the interaction network evolves, reflecting adjustments in ligand positioning and protein flexibility that stabilize the complex over time. Such dynamic interactions are consistent with the RMSD and Rg analyses, highlighting both the stability of the protein-ligand complex and the adaptive nature of binding within the active site.

Fig. 9

The secondary structure of the protein-ligand complex was examined utilizing the DSSP algorithm as executed in MDTraj [79,80]. The study retrieved the protein structures from the start (0 ns) and final (100 ns) images of the molecular dynamics trajectory. The DSSP assignments were derived directly from the PDB files, and the secondary structure composition was quantified by determining the relative percentages of residues in α-helix (H), β-sheet/extended strand (E), and coil (C) conformations. For comparative analysis, the DSSP findings were exported as text files and examined using bespoke Python programs that produced bar graphs (Fig. 10) of structural information at the two time points.

The DSSP analysis indicated that at the commencement of the simulation (0 ns), the protein consisted of approximately 49 % α-helices, 12 % β-sheets, and 39 % coil structures. Following 100 ns of simulation, the relative composition somewhat adjusted to around 46 % α-helices, 11 % β-sheets, and 43 % coils. These small shifts indicate that the global fold of TmpK was largely preserved throughout the trajectory, with no evidence of unfolding or destabilization. Minor fluctuations were observed in loop/coil regions, consistent with localized flexibility rather than global instability. Importantly, the Ser150–Glu170 loop, central to the proposed allosteric mechanism, remained predominantly in a coil conformation at both time points. While retaining its structural classification, this loop exhibited enhanced flexibility in RMSF profiles, supporting its role as a dynamic mediator of communication between the orthosteric and allosteric sites. Together, the DSSP, RMSD, and RMSF analyses demonstrate that TmpK maintains overall structural stability

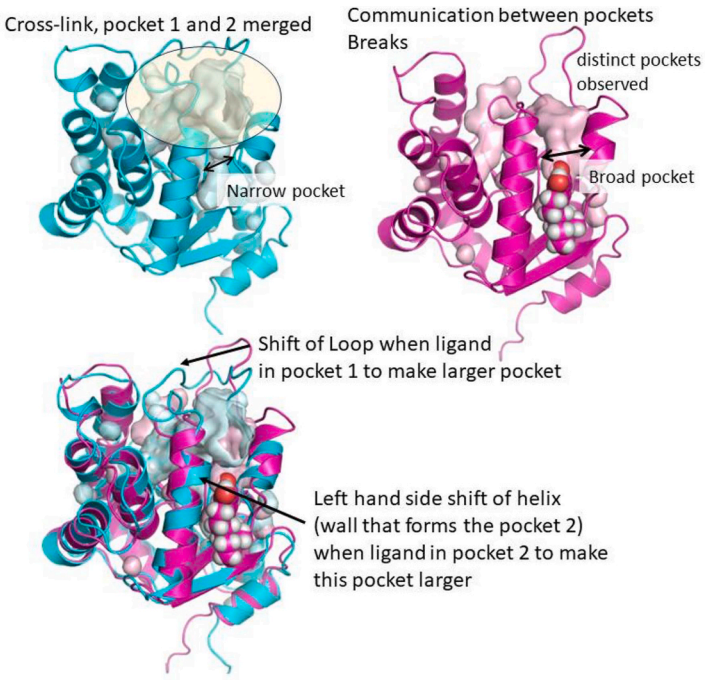

Fig. 6. Intramolecular cross-talk between active site (pocket 1) and allosteric site (pocket 2) during MD-simulation.

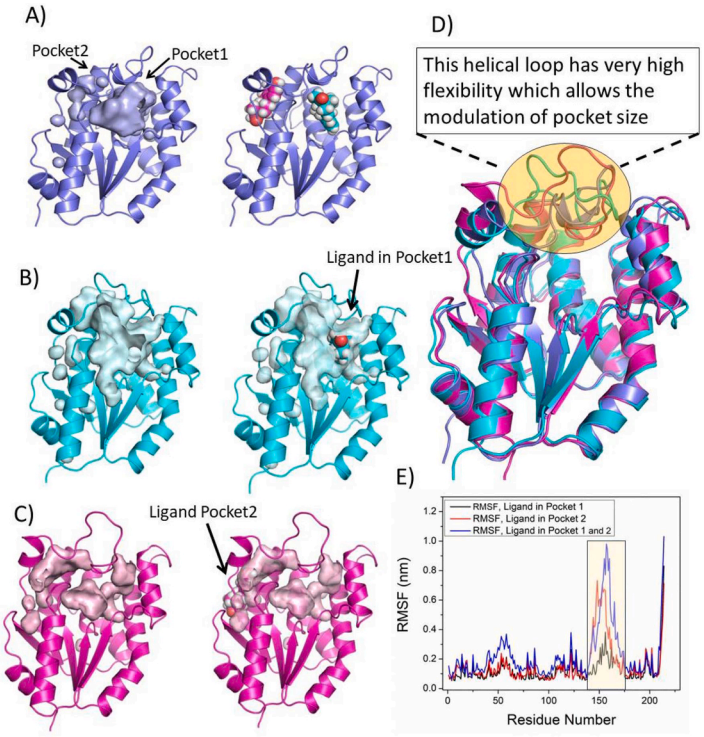

Fig. 7. The dynamics of allosteric and active site cavity in Thymidylate kinase. A) The two predicted pockets are shown in the modeled structure (pink shade), Pocket1 (active site pocket) and Pocket 2(allosteric pocket) are shown in the modelled structures. The ligands are shown in each of the pockets (right hand panel). B) The MD-simulated snapshot with ligand (4HY) in pocket1; the volume of pocket2 has decreased. C) The MD-simulated snapshot with ligand (4HY) in pocket2; the volume of pocket1 has decreased significantly. D) The snapshots of Figures in Panel B and D are superimposed, Ser150-Glu170 is a short stretch of loop which is highly flexible and responsible for cavity volume modulation between pocket1 and 2. E) The Root Mean Square Fluctuation (RMSF) value shows high fluctuation in the Ser150-Glu170 loop region.

during ligand binding, while localized flexibility in the Ser150–Glu170 loop enables the conformational adaptability necessary for allosteric regulation.

In addition to the global RMSD estimations, loop-specific RMSD analysis were performed for the Ser150–Glu170 loop, which is pivotal to the suggested allosteric mechanism. The backbone RMSD stabilized between 0.3 and 0.45 nm for systems 1 and 2, whereas the loop had greater oscillations (0.4 to 0.6 nm), aligning with its function as a

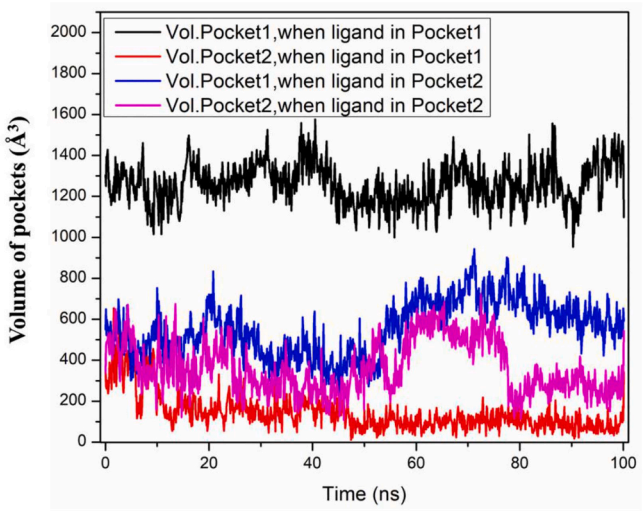

Fig. 8. The allosteric and active site pocket volumes during MD-simulation studies.

flexible conduit for inter-pocket communication. This localized mobility supports the RMSF findings and highlights the functional significance of the loop in volume modulation.

The stability of TmpK's secondary structure was assessed using DSSP assignments throughout the 100 ns trajectory. The global fold was maintained, with α-helices (49 % → 46 %) and β-sheets (12 % → 11 %) exhibiting relatively negligible alterations, but coil fractions experienced a modest rise (39 % → 43 %). The Ser150–Glu170 loop consistently maintained a coil shape during the simulation, demonstrating that structural integrity was preserved while localized flexibility enabled dynamic pocket reconfiguration.

To verify the adequacy of the 100 ns production run after 10 ns equilibration, convergence was evaluated using block averaging of RMSD and Rg across 10 ns intervals. Both measurements attained stable plateaus after around 40 ns and maintained consistency thereafter, thereby validating sufficient conformational sampling. While extended timeframes may reveal further gradual shifts, the documented stabilization of RMSD/Rg and consistent variation in pocket volumes indicate that the selected timescale adequately encapsulates the fundamental dynamics of TmpK's allosteric communication.

Ultimately, pocket volume investigations demonstrated asymmetric modulation of the orthosteric and allosteric cavities contingent upon ligand occupancy. The binding of 4HY to pocket 1 enlarged the orthosteric site while decreasing the volume of the allosteric cavity, whereas the occupancy of pocket 2 produced the contrary effect. The results, along with RMSD, RMSF, and DSSP investigations, underscore the pivotal function of the Ser150–Glu170 loop as a dynamic facilitator of allosteric signaling, while affirming the protein's structural stability under simulated settings.

To examine the structural communication between the active and allosteric sites of the protein-ligand complex without molecular dynamics trajectory data, we utilized a combined distance-difference and Anisotropic Network Model (ANM)-based correlation method, relying on the initial and final protein structures [81,82].

Fig. 11(a) illustrates the Δ distance between active and allosteric residues. This heatmap illustrates the variation in inter-residue distances between the active-site residues (Y-axis) and allosteric-site residues (X-axis) throughout the simulation period. Red sections denote residues that experienced significant positional deviation (substantial structural rearrangement), while blue regions signify little alteration. The prominent red area in the lower portion indicates that a particular active-site sub-segment is acutely responsive to allosteric binding, aligning with the notion of long-range communication between the pockets. The ANM Correlation (End State) shown in Fig. 11(d) presents the residue-motion correlation matrix obtained from the Anisotropic Network Model (ANM) at the conclusion of the simulation. Positive correlations (red) signify residues that exhibit cooperative, synchronous movements, whereas negative correlations (blue) denote anti-correlated motions (opposing orientations). Upon conclusion of the simulation, pockets exhibit disturbed and dispersed correlation patterns, indicative of allosteric disturbance in the collective motions. The ANM Correlation (Start State) shown in Fig. 11(c) displays the correlation matrix at the first conformation. The active-site and allosteric residues demonstrate a more continuous and coherent correlation network (predominantly red and light shades), suggesting that prior to ligand influence, both pockets operate in a coordinated fashion as components of a cohesive dynamic system. Fig. 11(d) illustrated the Δ correlation between Active and Allosteric (End − Start). This heatmap illustrates the net variation in

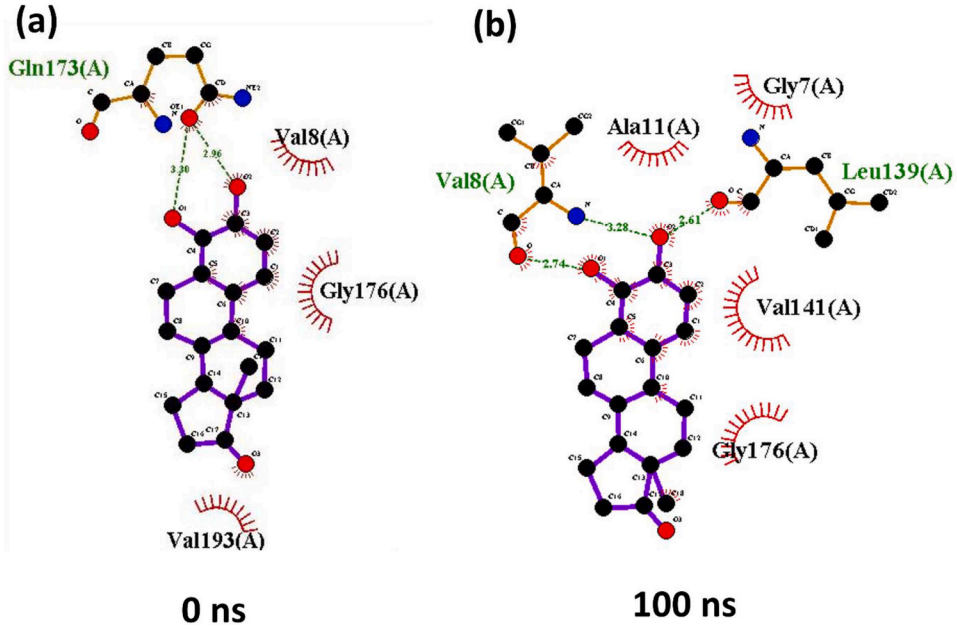

Fig. 9. 2D Interaction analysis of the 0 ns and 100 ns during MD simulation Pocket1 (active site pocket).

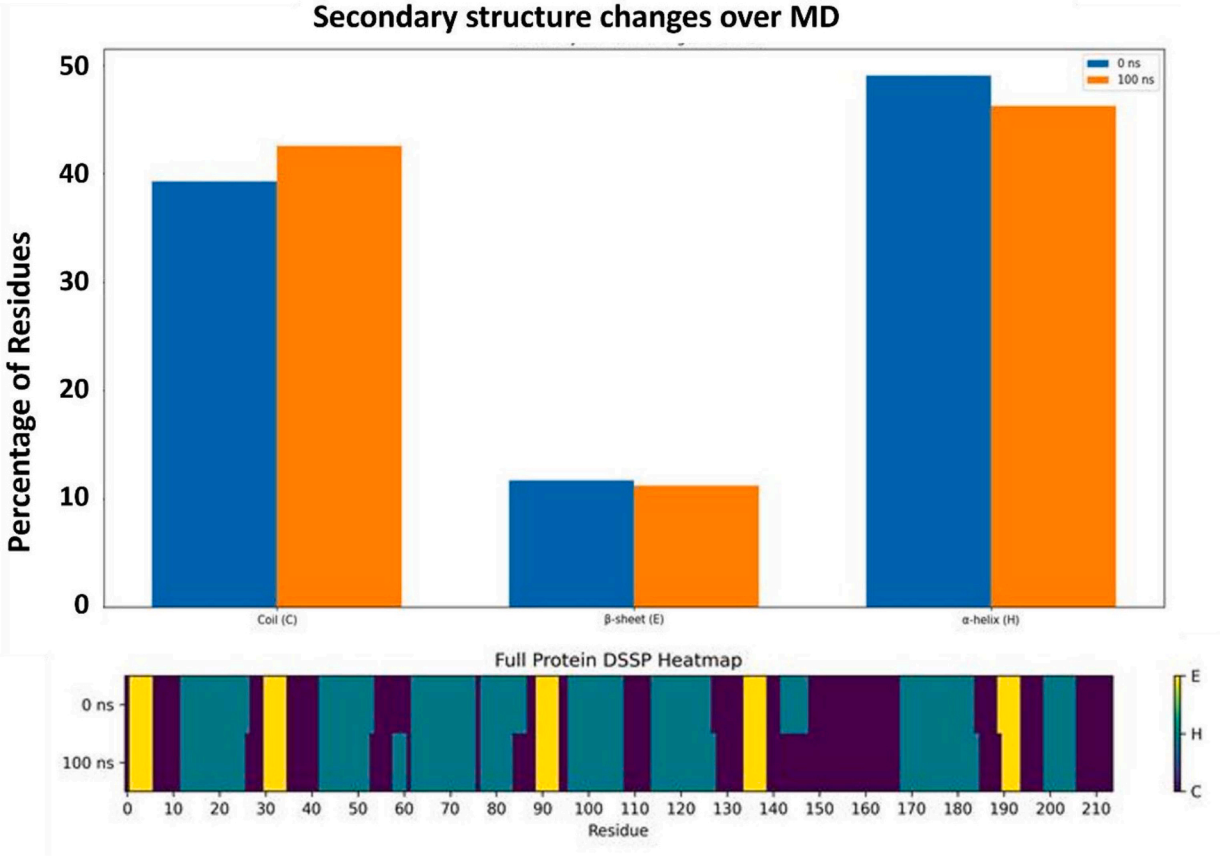

Fig. 10. DSSP Secondary structure content during MD simulation.

motion correlations between initial and final states. Red areas signify freshly established or enhanced correlations, whilst blue areas denote diminished correlations or weakened communication pathways. The existence of extensive blue areas indicates that allosteric binding disrupts established communication pathways, thereby modifying the dynamic network of pockets, which is characteristic of allosteric regulation.

The ANM correlation study revealed a robust positive coupling in the initial structure, which significantly diminished or restructured in the final state, as indicated by the end-correlation and Δ-correlation maps. Collectively, these findings suggest that ligand binding triggers a selective, pathway-specific allosteric communication alteration instead of a comprehensive structural transformation, hence reinforcing the existence of a targeted allosteric signaling network between the two sites.

4. Discussion

Allostery is a fundamental regulatory mechanism in biological systems, allowing proteins, particularly enzymes, to undergo conformational changes upon the binding of effector molecules at sites distinct from the active site. In the context of *Mycobacterium tuberculosis* (Mtb), allosteric modulation represents an attractive strategy for therapeutic intervention, as it can effectively disrupt enzymatic functions essential for bacterial survival and replication. Given the increasing prevalence of multidrug-resistant tuberculosis (MDR-TB) and extensively drug-resistant tuberculosis (XDR-TB), targeting allosteric sites provides a compelling alternative to traditional orthosteric inhibitors, which are often rendered ineffective due to resistance-associated mutations [83]. Molecular dynamics (MD) simulations have become indispensable tools for probing allosteric communication in proteins [84]. One of the key challenges in computational modeling of allosteric sites lies in their inherent flexibility and cryptic nature, which often makes them difficult to detect in the absence of a bound ligand [85]. Unlike orthosteric sites, which are typically well-defined and rigid, allosteric pockets exhibit significant conformational plasticity, complicating structure-based drug design efforts.

Our study explores the role of allosteric modulation in *Mycobacterium tuberculosis* thymidylate kinase (TmpK), highlighting how ligand binding at different sites can influence enzyme activity. Through virtual screening and molecular docking, we identified 4-Hydroxyestrone (4HY) as a potential molecule that interacts with both the allosteric and orthosteric sites, with docking scores of −11.5 kcal/mol and −7.1 kcal/mol, respectively. 4HY (FoodDatabase (FOODDB) Primary ID: FDB023786), a naturally occurring catechol estrogen and a minor metabolite of estrone (E1) and 17β-estradiol (E2), is known for its minimal estrogenic activity. Though the levels were not exactly quantified, it may be expected to be found in wide range of animal/avian derived food products [https://foodb.ca/compounds/FDB02378]. Interestingly, it has also been reported to exhibit neuroprotective effects by promoting p53 deacetylation through SIRT1, which enhances cellular resistance to oxidative stress [73]. Beyond its direct interaction with TmpK as predicted in this study, 4HY is also been known as an inhibitor of protein disulfide isomerase (PDI) and a modulator of ferroptosis in the host [86].

Recent investigations have identified numerous potential scaffolds that target Mtb-TMK. El-Shoukrofy et al. engineered and synthesized two series of tetrahydropyrimidine (THPM)–1,2,3-triazole hybrid compounds, exhibiting inhibitory activity akin to the natural substrate deoxythymidine monophosphate (dTMP) [87]. Venugopala et al. found 3-cyanopyridones and 1,6-naphthyridin-2-ones as effective Mtb-TMK inhibitors using computer-aided screening, subsequently validating their whole-cell anti-TB efficacy against both H37Rv and MDR strains

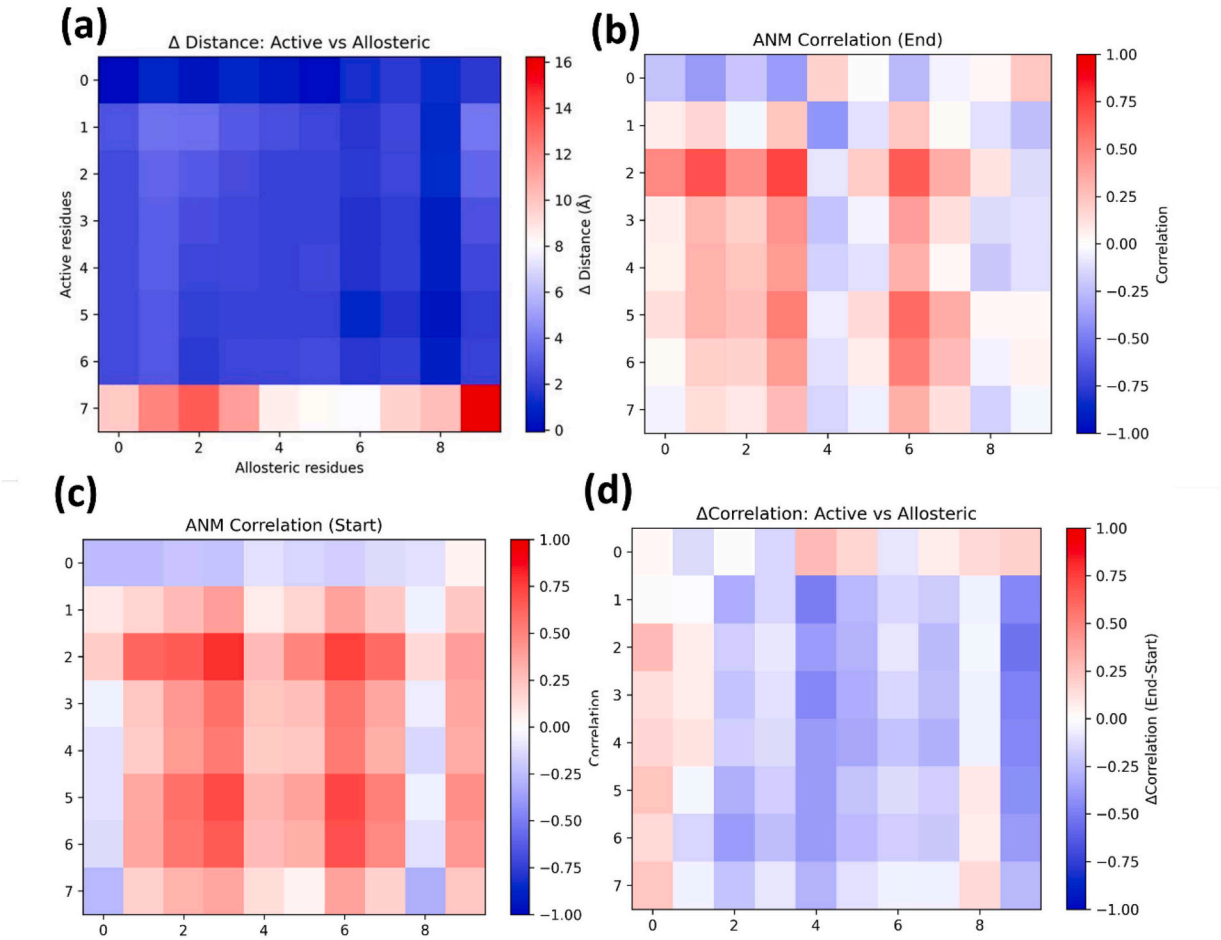

Fig. 11. Dynamic coupling between active and allosteric residues. (a) Δ-distance heatmap shows long-range structural rearrangements between active and allosteric residues upon ligand binding. **(b–c)** ANM correlation matrices at the end vs. start state reveal disruption of collective motions. **(d)** Δ-correlation highlights the loss of pocket–pocket communication, supporting an allosteric regulatory effect.

[88]. In alignment with these results, an additional biochemical and NMR-based fragment screening initiative identified 3-cyanopyridones and 1,6-naphthyridin-2-ones as novel chemotypes with the ability to inhibit Mtb-TMK [89]. Furthermore, several sugar-modified thymidine analogues have been documented to interact with TMPK by unique mechanisms, including a new category of bicyclic nucleosides and a dinucleoside, which represent some of the most selective TMPK inhibitors discovered thus far [90]. These investigations underscore the continuous pursuit of chemically varied Mtb-TMK inhibitors, especially concentrating on orthosteric site interaction. Conversely, our research reveals 4-hydroxyestrone (4HY) as a distinctive non-nucleoside entity that can bind at both the orthosteric site and a remote allosteric pocket, thereby providing a new mechanism for enzyme control. Our analysis enhances the existing framework of Mtb-TMK inhibitor design by elucidating the long-range communication between these pockets and emphasizes the promise of allosteric or bitopic compounds in forthcoming anti-TB treatments.

The outcomes of this study support the notion that a strong therapeutic intervention framework can be developed by focusing on allosteric communication in TmpK. The dependency of ligand binding and structural flexibility is highlighted by the dynamic modulation between orthosteric and allosteric sites, especially in the Ser150–Glu170 loop region. Comparable findings have been shown for various kinases and nucleotide-binding enzymes, wherein loop flexibility promotes allosteric communication and conformational transitions [91,92]. This corroborates the premise that the found allosteric region is functionally significant and amenable to pharmacological targeting.

The instability evident in the dual-ligand MD simulations suggests that concurrent unlinked binding at both sites may be disadvantageous in physiological settings. This indicates the need for rationally designed bitopic ligands that are covalently bonded to stabilize dual-site occupancy by integrating orthosteric and allosteric pharmacophores [75]. Bitopic techniques have been effective in the identification of GPCR medicines, improving both selectivity and potency [93]. The prospect of a novel frontier in anti-TB drug creation may be realized by applying such methodologies to TmpK.

Our RMSF analysis underscores the biological importance of the Ser150–Glu170 loop, which is further supported by evolutionary conservation. The conservation of critical residues in the sequence alignment of TmpK among pathogenic mycobacterial species suggests that the regulatory function of TmpK is conserved [27,28,50]. This renders the loop a persuasive foundation for subsequent inhibitor tailoring. Additionally, in order to improve selectivity and mitigate off-target effects, it is imperative to implement additional medicinal chemistry modifications, as 4-hydroxyestrone (4HY) is a well-established estrogenic molecule that has an impact on a variety of cellular targets [27,50]. Increased fluctuations in this loop, as observed in root mean square fluctuation (RMSF) analysis, further highlight its role in allosteric regulation. These findings provide compelling evidence that TmpK undergoes ligand-induced conformational changes that modulate enzymatic function, reinforcing the potential of allosteric inhibitors [94].

The significance of allosteric targeting extends beyond TmpK. Previous studies have demonstrated that allosteric modulators can overcome resistance mechanisms that frequently arise in orthosteric drug

targets [95]. Unlike traditional inhibitors, which are prone to resistance due to mutations in the active site, allosteric inhibitors target distinct regulatory regions that are less susceptible to evolutionary pressure. The recent examples are the discovery of Pranlukast, an allosteric inhibitor of Mtb Ornithine acetyltransferase (MtArgJ), which simultaneously targets intracellular bacteria and host pro-survival signaling pathways [96], targeting the allosteric mechanism governing aspartate kinase from the *Wolbachia* endosymbiont of *Brugia malayi* (WBm) has demonstrated potential for structure-based drug discovery aimed at overcoming drug resistance in lymphatic filariasis [97]. Additionally, studies on Lim kinases specifically LIMK1-YFYW and LIMK2-WFVW, have opened avenues for the development of selective allosteric inhibitors that modulate actin dynamics, offering promising strategies to combat cancer-related processes [98].

The concept of bitopic ligands, which engage both orthosteric and allosteric sites within a single molecule, has emerged as a promising strategy for drug design [99,100]. Such ligands have been extensively explored in G protein-coupled receptor (GPCR) research, where they have demonstrated enhanced specificity and efficacy compared to conventional drugs [75]. In the context of tuberculosis treatment, bitopic ligands could provide dual-site engagement, that stabilize key interactions while maintaining selectivity. This approach has the potential to enhance drug efficacy, reduce required dosages, and minimize the likelihood of resistance development.

Beyond TmpK, extending computational analysis to other essential Mtb enzymes could uncover additional cryptic allosteric sites and reveal new avenues for therapeutic intervention. Advanced structure-based drug design techniques, such as molecular fragment screening, machine learning-driven virtual screening, and free energy perturbation (FEP) calculations, could further refine the identification and optimization of allosteric inhibitors. The integration of computational and experimental approaches, including X-ray crystallography, cryo-EM, and biophysical binding assays, will be essential for validating predicted allosteric sites and translating these findings into clinically viable therapeutics.

This investigation improves the structural and mechanistic understanding of TmpK allostery and provides a proof-of-concept for the application of allosteric control in bacterial enzymes. The proposed bitopic ligand method, which combines orthosteric and allosteric targeting, has the potential to resolve the deficiencies of current anti-TB medications. The experimental validation of the proposed allosteric pocket, the production of interconnected bitopic inhibitors, and the assessment of their therapeutic efficacy against multidrug-resistant tuberculosis will be the primary focus of future endeavors.

4.1. Experimental validation and future applications

This research establishes a computational basis for the dual-site binding mechanism of 4-Hydroxyestrone (4HY) with Thymidylate Kinase (TMK). A systematic future experimental validation workflow has been developed to translate these results into empirically proven outputs as shown in Fig. 12. The workflow comprises four sequential stages: (i) Biochemical validation through enzymatic inhibition assays to quantify catalytic turnover and IC_{50} values; (ii) Biophysical characterization utilizing differential scanning fluorimetry (DSF) for ligand-induced stabilization and ITC/SPR for measuring binding affinity and stoichiometry; (iii) Site-directed mutagenesis to verify the functional significance of the predicted allosteric pocket; and (iv) Lead refinement employing structure-guided design, pharmacophore optimization, and linker engineering to produce bitopic derivatives with enhanced selectivity. Simultaneous in silico off-target filtering and iterative ADMET screening will be employed to reduce interactions with proteins like PDI and SIRT1. This study integrates computational insights with a systematic validation procedure, thereby delineating a definitive translational pathway for the creation of selective, mechanistically validated dual-site TMK inhibitors.

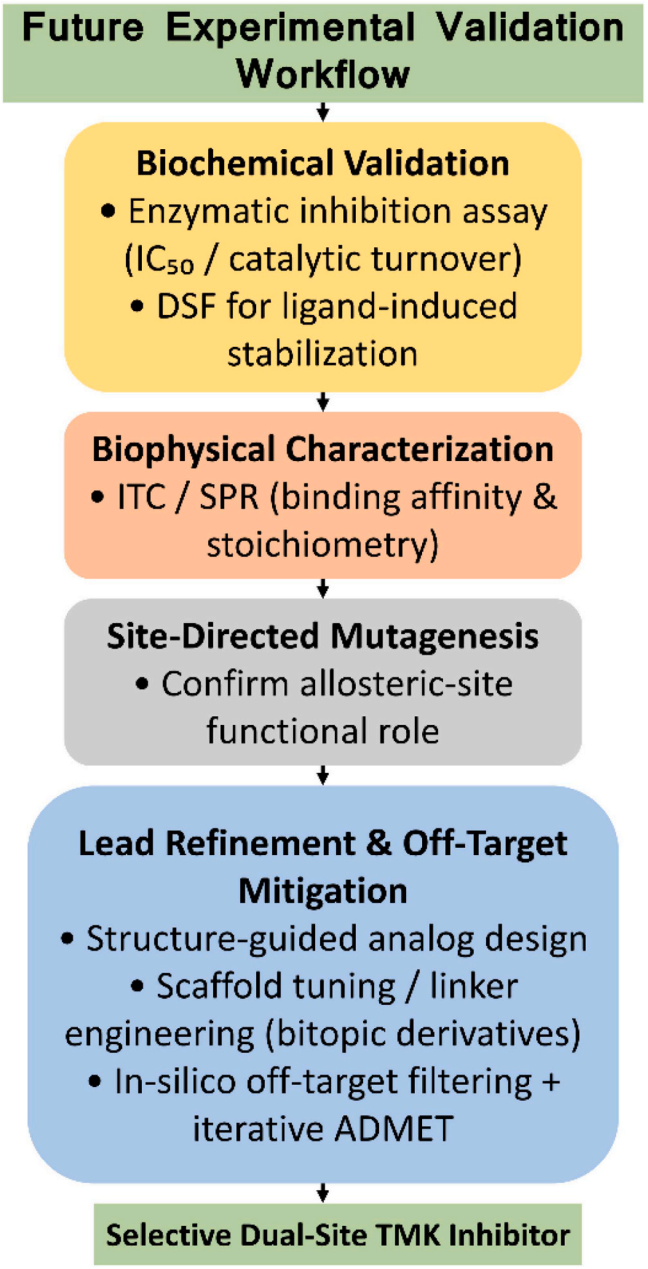

Fig. 12. Future experimental validation workflow.

5. Conclusion

In summary, our study sheds light on the allosteric regulation of TmpK and introduces a computational framework for structure-based drug discovery. By uncovering the functional link between orthosteric and allosteric binding sites, we highlight the potential of allosteric inhibitors and bitopic ligands as promising avenues for tackling multidrug-resistant tuberculosis. These findings lay the groundwork for future research, bringing us one step closer to next-generation anti-tuberculosis therapeutics.

Funding source

This study does not receive any funding.

CRediT authorship contribution statement

Amsaveni Sivaprakasam: Writing – original draft, Visualization, Validation, Software, Project administration, Methodology, Investigation, Formal analysis, Data curation, Conceptualization. **Radha Mahendran:** Writing – review & editing, Visualization, Validation, Supervision, Software, Methodology, Data curation. **Umashankar Vetrivel:** Writing – review & editing, Visualization, Validation, Supervision, Investigation, Conceptualization. **Luke Elizabeth Hanna:** Writing – review & editing, Validation, Supervision.

Declaration of competing interest

The authors declare that they have no known competing financial interests or personal relationships that could have appeared to influence the work reported in this paper.

Acknowledgments

Authors are thankful to the Vels Institute of Science, Technology and Advanced Studies (VISTAS) for infrastructure and facilities.

Supplementary materials

Supplementary material associated with this article can be found, in the online version, at doi:10.1016/j.rineng.2025.108719.

Data availability

Data will be made available on request.

References

[1] Global tuberculosis report, World Health Organization; 2024, Licence: CC BY-NC-SA 3.0 IGO, Geneva, 2024.
[2] W. Bai, E.K. Ameyaw, Global, regional and national trends in tuberculosis incidence and main risk factors: a study using data from 2000 to 2021, BMC. Public Health 24 (1) (2024 Jan 2) 12, https://doi.org/10.1186/s12889-023-17495-6. PMID: 38166735; PMCID: PMC10759569.
[3] D. Vishwakarma, A. Gaidhane, S. Sahu, A.S. Rathod, Multi-Drug Resistance Tuberculosis (MDR-TB) Challenges in India: a Review, Cureus 15 (12) (2023 Dec 9) e50222, https://doi.org/10.7759/cureus.50222. PMID: 38192967; PMCID: PMC10772311.
[4] K.J. Seung, S. Keshavjee, M.L. Rich, Multidrug-Resistant Tuberculosis and Extensively Drug-Resistant Tuberculosis, Cold. Spring. Harb. Perspect. Med. 5 (9) (2015 Apr 27) a017863, https://doi.org/10.1101/cshperspect.a017863. PMID: 25918181; PMCID: PMC4561400.
[5] K.A. Alene, H. Yi, K. Viney, E.S. McBryde, K. Yang, L. Bai, D.J. Gray, A.C. A. Clements, Z. Xu, Treatment outcomes of patients with multidrug-resistant and extensively drug resistant tuberculosis in Hunan Province, China, BMC. Infect. Dis. 17 (1) (2017 Aug 16) 573, https://doi.org/10.1186/s12879-017-2662-8. PMID: 28814276; PMCID: PMC5559784.
[6] X. Zhang, R. Zhao, Y. Qi, X. Yan, G. Qi, Q. Peng, The progress of *Mycobacterium tuberculosis* drug targets, Front. Med. 11 (2024 Oct 21) 1455715, https://doi.org/10.3389/fmed.2024.1455715. PMID: 39497852; PMCID: PMC11533868.
[7] Z.S. Bhat, M.A. Rather, M. Maqbool, Z. Ahmad, Drug targets exploited in Mycobacterium tuberculosis: pitfalls and promises on the horizon, Biomed. PharmacOther 103 (2018 Jul) 1733–1747, https://doi.org/10.1016/j.biopha.2018.04.176. PMID: 29864964.
[8] H. Ando, Y. Kondo, T. Suetake, E. Toyota, S. Kato, T. Mori, T. Kirikae, Identification of katG mutations associated with high-level isoniazid resistance in Mycobacterium tuberculosis, Antimicrob. Agents Chemother. 54 (5) (2010 May) 1793–1799, https://doi.org/10.1128/AAC.01691-09. Epub 2010 Mar 8. PMID: 20211896; PMCID: PMC2863633.
[9] N. Dookie, S. Rambaran, N. Padayatchi, S. Mahomed, K. Naidoo, Evolution of drug resistance in Mycobacterium tuberculosis: a review on the molecular determinants of resistance and implications for personalized care, J. Antimicrob. Chemother 73 (5) (2018) 1138–1151, https://doi.org/10.1093/jac/dkx506.
[10] M. Serajian, C. Testagrose, M. Prosperi, et al., A comparative study of antibiotic resistance patterns in *Mycobacterium tuberculosis*, Sci. Rep. 15 (2025) 5104, https://doi.org/10.1038/s41598-025-89087-w.
[11] M.H. Hazbón, M. Brimacombe, M. Bobadilla del Valle, M. Cavatore, M. I. Guerrero, M. Varma-Basil, H. Billman-Jacobe, C. Lavender, J. Fyfe, L. García-García, C.I. León, M. Bose, F. Chaves, M. Murray, K.D. Eisenach, J. Sifuentes-Osornio, M.D. Cave, A. Ponce de León, D. Alland, Population genetics study of isoniazid resistance mutations and evolution of multidrug-resistant mycobacterium tuberculosis, Antimicrob. Agents Chemother. 50 (8) (2006 Aug) 2640–2649, https://doi.org/10.1128/AAC.00112-06. PMID: 16870753; PMCID: PMC1538650.
[12] F. Meacci, G. Orrù, E. Iona, F. Giannoni, C. Piersimoni, G. Pozzi, L. Fattorini, M. R Oggioni, Drug resistance evolution of a Mycobacterium tuberculosis strain from a noncompliant patient, J. Clin. Microbiol. 43 (7) (2005 Jul) 3114–3120, https://doi.org/10.1128/JCM.43.7.3114-3120.2005. PMID: 16000422; PMCID: PMC1169130.
[13] M.V. Shulgina, Mechanisms of mycobacterium tuberculosis drug resistance, Mol. Genet., Microbiol. Virol. 39 (2024) 1–13.
[14] R. Nussinov, C.J. Tsai, The different ways through which specificity works in orthosteric and allosteric drugs, Curr. Pharm. Des. 18 (9) (2012) 1311–1316, https://doi.org/10.2174/138161212799436377. PMID: 22316155; PMCID: PMC7458136.
[15] A. Christopoulos, Allosteric binding sites on cell-surface receptors: novel targets for drug discovery, Nat. Rev. Drug Discov. 1 (2002) 198–210, https://doi.org/10.1038/nrd746.
[16] C.J. Wenthur, P.R. Gentry, T.P. Mathews, C.W. Lindsley, Drugs for allosteric sites on receptors, Annu. Rev. Pharmacol. Toxicol. 54 (2014) 165–184, https://doi.org/10.1146/annurev-pharmtox-010611-134525. Epub 2013 Oct 2. PMID: 24111540; PMCID: PMC4063350.
[17] I.R. Svechkareva, A.S. Kolbin, Prospects for the use of allosteric drugs in real-world clinical practice, Real-World Data Evid. 3 (4) (2023) 15–21, https://doi.org/10.37489/2782-3784-myrwd-43. RussEDN: FJVVUX.
[18] D. Ni, Y. Li, Y. Qiu, J. Pu, S. Lu, J. Zhang, Combining allosteric and orthosteric drugs to overcome drug resistance, Trends. Pharmacol. Sci. 41 (5) (2020) 336–348, https://doi.org/10.1016/j.tips.2020.02.001.
[19] E. Barresi, C. Martini, F. Da Settimo, G. Greco, S. Taliani, C. Giacomelli, M. L Trincavelli, Allosterism vs. orthosterism: recent findings and future perspectives on A_2B AR physio-pathological implications, Front. Pharmacol. 12 (2021) 652121, https://doi.org/10.3389/fphar.2021.652121.
[20] V.R. Mingione, Allosteric regulation and inhibition of protein kinases, F1000Res. 12 (2023) 36794774, https://doi.org/10.12688/f1000research.36794.1.
[21] A.N. Lane, Regulation of mammalian nucleotide metabolism and its implications in disease, J. Cell Biochem. 116 (11) (2015) 2493–2501, https://doi.org/10.1002/jcb.25160.
[22] L. Zhang, J. Wei, Z. Zou, et al., RNA modification systems as therapeutic targets, Nat. Rev. Drug Discov. 24 (12) (2025) 789–804, https://doi.org/10.1038/s41573-025-01280-8.
[23] B. Petrova, A.G. Maynard, P. Wang, N. Kanarek, Regulatory mechanisms of onecarbon metabolism enzymes, J. Biol. Chem. 299 (12) (2023) 105457, https://doi.org/10.1016/j.jbc.2023.105457.
[24] J. Xie, G. Pan, L. Lai, Sequence and structure-based prediction of allosteric sites, J. Mol. Biol. 437 (20) (2025) 169305, https://doi.org/10.1016/j.jmb.2025.169305.
[25] F. Hu, F. Chang, L. Tao, X. Sun, L. Liu, Y. Zhao, Z. Han, C. Li, Prediction of protein allosteric sites with transfer entropy and spatial neighbor-based evolutionary information learned by an ensemble model, J. Chem. Inf. Model. 64 (15) (2024) 6197–6204, https://doi.org/10.1021/acs.jcim.4c00544.
[26] D. Ni, J. Wei, X. He, A.U. Rehman, X. Li, Y. Qiu, J. Pu, S. Lu, J. Zhang, Discovery of cryptic allosteric sites using reversed allosteric communication by a combined computational and experimental strategy, Chem. Sci. 12 (1) (2020) 464–476, https://doi.org/10.1039/d0sc05131d.
[27] R.V. Chikhale, S.P. Pawar, M.S. Kolpe, O.D. Shinde, K.A. Dahlous, S. Mohammad, P.C. Patil, S. Bhowmick, Identification of mycobacterial Thymidylate kinase inhibitors: a comprehensive pharmacophore, machine learning, molecular docking, and molecular dynamics simulation studies, Mol. Divers. 28 (4) (2024) 1947–1964, https://doi.org/10.1007/s11030-024-10967-w.
[28] H.A. Abou-Zied, Emerging insights into pyrazoline motifs: a comprehensive review on their therapeutic potential, Bioorg. Chem. 115 (2024) 105062, https://doi.org/10.1016/j.bioorg.2023.105062.
[29] S.K. Suvaiv, S.M. Hasan, S.P. Kushwaha, S.M.H. Zaidi, A. Kumar, M. Shahanawaz, Structure-guided development of mycobacterial thymidine monophosphate kinase (MtbTMPK) inhibitors: unlocking new frontiers in tuberculosis research, Curr. Top. Med. Chem. 25 (10) (2025) 1–12, https://doi.org/10.2174/0115680266372955250514075248.
[30] A. Haouz, F. Dardel, J. Poncet, et al., Enzymatic and structural analysis of inhibitors designed to target Mycobacterium tuberculosis thymidine monophosphate kinase, Biochimie 85 (3) (2003) 267–276, https://doi.org/10.1016/S0021-9258(03)00004-2.
[31] J. Huang, Recent advances in computational strategies for allosteric site prediction, Comput. Struct. Biotechnol. J. 23 (2025) 1234–1245, https://doi.org/10.1016/j.csbj.2025.02.014.
[32] R. Zhu, C. Wu, J. Zha, S. Lu, J. Zhang, Decoding allosteric landscapes: computational methodologies for enzyme modulation and drug discovery, RSC. Chem. Biol. 6 (2025) 539–554, https://doi.org/10.1039/D4CB00282B.
[33] O. Sheik Amamuddy, W. Veldman, C. Manyumwa, A. Khairallah, S. Agajanian, O. Oluyemi, G.M. Verkhivker, Tastan Bishop Ö. Integrated computational approaches and tools for allosteric drug discovery, Int. J. Mol. Sci. 21 (3) (2020) 847, https://doi.org/10.3390/ijms21030847.
[34] B. Siddiqui, C.S. Yadav, M. Akil, M. Faiyyaz, A.R. Khan, N. Ahmad, F. Hassan, M. I. Azad, M. Nasibullah, I. Azad, Artificial intelligence in computer-aided drug design (CADD) tools for the finding of potent biologically active small molecules: traditional to modern approach, Comb. Chem. High. Throughput. Screen. 28 (1) (2025) 1–15, https://doi.org/10.2174/0113862073334062241015043343.

[35] V. Lamba, I. Ghosh, New directions in targeting protein kinases: focusing upon true allosteric and bivalent inhibitors, Curr. Pharm. Des. 18 (20) (2012) 2936–2945, https://doi.org/10.2174/138161212800672813.
[36] L. Song, R. Merceron, F. Hulpia, et al., Structure-aided optimization of non-nucleoside M. tuberculosis TmpKinhibitors, Eur. J. Med. Chem. 225 (2021) 113784, https://doi.org/10.1016/j.ejmech.2021.113784.
[37] Y. Jian, M.D.P. Risseeuw, M. Froeyen, et al., 1-(Piperidin-3-yl)thymine amides as inhibitors of *M. tuberculosis* thymidylate kinase, J. Enzyme Inhib. Med. Chem. 34 (1) (2019) 1730–1739, https://doi.org/10.1080/14756366.2019.1662790.
[38] S. Van Calenbergh, Structure-aided design of inhibitors of Mycobacterium tuberculosis thymidylate kinase, Verh. K. Acad. Geneeskd. Belg. 68 (4) (2006) 223–248.
[39] O. Familiar, H. Munier-Lehmann, A. Negri, et al., Exploring acyclic nucleoside analogues as inhibitors of Mycobacterium tuberculosis thymidylate kinase, ChemMedChem. 3 (7) (2008) 1083–1093, https://doi.org/10.1002/cmdc.200800060.
[40] S. Konate, K.N.P.G. Allangba, I. Fofana, et al., Improved inhibitors targeting the thymidylate kinase of multidrug-resistant *mycobacterium tuberculosis* with favorable pharmacokinetics, Life 15 (2) (2025) 173, https://doi.org/10.3390/life15020173. Published 2025 Jan 25.
[41] O. Bulvas, Z. Knejzlík, J. Sýs, et al., Deciphering the allosteric regulation of mycobacterial inosine-5′-monophosphate dehydrogenase, Nat. Commun. 15 (2024) 6673, https://doi.org/10.1038/s41467-024-50933-6.
[42] S. Günther, P.Y.A. Reinke, Y. Fernández-García, J. Lieske, T.J. Lane, H.M. Ginn, et al., X-ray screening identifies active site and allosteric inhibitors of SARS-CoV-2 main protease, Science 1979 372 (6542) (2021 May 7) 642–646, https://doi.org/10.1126/science.abf7945. PMID: 33811162; PMCID: PMC8224385.
[43] A. Fatima, A.M. Geethakumari, W.S. Ahmed, K.H. Biswas, A potential allosteric inhibitor of SARS-CoV-2 main protease (M^{pro}) identified through metastable state analysis, Front. Mol. Biosci. 11 (2024 Sep 6) 1451280, https://doi.org/10.3389/fmolb.2024.1451280. PMID: 39310374; PMCID: PMC11413593.
[44] A.-M. AF, Allosteric modulators: an emerging concept in drug discovery, ACS. Med. Chem. Lett. 6 (2) (2015 Jan 8) 104–107, https://doi.org/10.1021/ml5005365. PMID: 25699154; PMCID: PMC4329591.
[45] T.J. El-Baba, C.A. Lutomski, A.L. Kantsadi, T.R. Malla, T. John, V. Mikhailov, J. R. Bolla, C.J. Schofield, N. Zitzmann, I. Vakonakis, C.V. Robinson, Allosteric inhibition of the SARS-CoV-2 main protease: insights from mass spectrometry based assays*, Angew. Chem. Int. Ed. Engl. 59 (52) (2020 Dec 21) 23544–23548, https://doi.org/10.1002/anie.202010316. Epub 2020 Oct 15. PMID: 32841477; PMCID: PMC7461284.
[46] M. Mori, S. Villa, S. Ciceri, D. Colombo, P. Ferraboschi, F. Meneghetti, An outline of the latest crystallographic studies on inhibitor-enzyme complexes for the design and development of new therapeutics against tuberculosis, Molecules. 26 (23) (2021) 7082, https://doi.org/10.3390/molecules26237082. Published 2021 Nov 23.
[47] Y. Jian, R. Merceron, S. De Munck, et al., Endeavors towards transformation of M. tuberculosis thymidylate kinase (MtbTMPK) inhibitors into potential antimycobacterial agents, Eur. J. Med. Chem. 206 (2020) 112659, https://doi.org/10.1016/j.ejmech.2020.112659.
[48] Z.A. Bhat, D. Chitara, J. Iqbal, B.S. Sanjeev, A. Madhumalar, Targeting allosteric pockets of SARS-CoV-2 main protease M(pro), J. Biomol. Struct. Dyn. 40 (2022) 6603–6618.
[49] M. Yuce, E. Cicek, T. Inan, A.B. Dag, O. Kurkcuoglu, F.A. Sungur, Repurposing of FDA-approved drugs against active site and potential allosteric drug-binding sites of COVID-19 main protease, Proteins 89 (2021) 1425–1441, https://doi.org/10.1002/prot.26164.
[50] S. Sukumar, A. Krishman, M.K. Khan, Protein kinases as antituberculosis targets: the case of thymidylate kinases, Front. Biosci. Landmark. Ed. 25 (9) (2020) 1636–1654, https://doi.org/10.2741/4871.
[51] Wu N., Strömich L., Yaliraki S.N. Prediction of allosteric sites and signaling: insights from benchmarking datasets. Patterns (N Y). 2021 Dec 9;3(1):100408. doi: 10.1016/j.patter.2021.100408. PMID: 35079717; PMCID: PMC8767309.
[52] L. Hong, H. Liang, W. Man, Y. Zhao, P. Guo, Estrogen and bacterial infection, Front. Immunol. 16 (2025) 1556683, https://doi.org/10.3389/fimmu.2025.1556683. Published 2025 Apr 29.
[53] J.S. Kim, Y.R. Kim, C.S. Yang, Host-Directed Therapy in Tuberculosis: targeting Host Metabolism, Front. Immunol. 11 (2020) 1790, https://doi.org/10.3389/fimmu.2020.01790. Published 2020 Aug 13.
[54] E.K. Jeong, H.J. Lee, Y.J. Jung, Host-Directed Therapies for Tuberculosis, Pathogens 11 (11) (2022) 1291, https://doi.org/10.3390/pathogens11111291. Published 2022 Nov 3.
[55] N.V. Simwela, E. Jaecklein, C.M. Sassetti, D.G. Russell, Impaired fatty acid import or catabolism in macrophages restricts intracellular growth of *Mycobacterium tuberculosis*, Elife 13 (2025) RP102980, https://doi.org/10.7554/eLife.102980. Published 2025 Mar 13.
[56] Z. Wu, R.M. Pfeiffer, D.A. Byrd, et al., Associations of circulating estrogens and estrogen metabolites with fecal and oral microbiome in postmenopausal women in the ghana breast health study, Microbiol. Spectr. 11 (4) (2023) e0157223, https://doi.org/10.1128/spectrum.01572-23.
[57] O. Trott, A.J. Olson, AutoDock Vina: improving the speed and accuracy of docking with a new scoring function, efficient optimization, and multithreading, J. Comput. Chem. 31 (2) (2010) 455–461, https://doi.org/10.1002/jcc.21334.
[58] C.M. Labbé, J. Rey, D. Lagorce, et al., MTiOpenScreen: a web server for structure-based virtual screening, Nucleic. Acids. Res. 43 (W1) (2015) W448–W454, https://doi.org/10.1093/nar/gkv306.
[59] H.M. Berman, J. Westbrook, Z. Feng, G. Gilliland, T.N. Bhat, H. Weissig, et al., The protein data bank, Nucleic. Acids. Res. 28 (1) (2000) 235–242, https://doi.org/10.1093/nar/28.1.235.
[60] M.N. Drwal, P. Banerjee, M. Dunkel, M.R. Wettig, R. Preissner, ProTox: a web server for the in silico prediction of rodent oral toxicity, Nucleic. Acids. Res. 10 (2014) 1–6.
[61] Johansson, M.U., Zoete V., Michielin O. & Guex N. (2012) Defining and searching for structural motifs using DeepView/Swiss-PdbViewer BMC Bioinformatics, 13: 173.
[62] G.M. Morris, R. Huey, W. Lindstrom, M.F. Sanner, R.K. Belew, D.S. Goodsell, A. J. Olson, AutoDock4 and AutoDockTools4: automated docking with selective receptor flexibility, J. Comput. Chem. 30 (2009) 2785–2791.
[63] M.J. Abraham, T. Murtola, R. Schulz, S. Páll, J.C. Smith, B. Hess, et al., GROMACS: high performance molecular simulations through multi-level parallelism from laptops to supercomputers, SoftwareX. 1–2 (2015) 19–25, https://doi.org/10.1016/j.softx.2015.06.001.
[64] J. Huang, A.D. MacKerell Jr., CHARMM36 all-atom additive protein force field: validation based on comparison to NMR data, J. Comput. Chem. 34 (25) (2013) 2135–2145, https://doi.org/10.1002/jcc.23354.
[65] K. Vanommeslaeghe, E. Prabhu Raman, A.D. MacKerell Jr., Automation of the CHARMM general force field (CGenFF) II: assignment of bonded parameters and partial atomic charges, J. Chem. Inf. Model. 52 (12) (2012) 3155–3168, https://doi.org/10.1021/ci3003649.
[66] A. Kazhiyev, S. Kaumbekova, D. Shah, Malic acid-based deep eutectic solvent and its application in insulin's structural stability, Results. Eng. 20 (2023) 101529, https://doi.org/10.1016/j.rineng.2023.101529.
[67] B. Hess, H. Bekker, H.J. Berendsen, J.G. Fraaije, LINCS: a linear constraint solver for molecular simulations, J. Comput. Chem. 18 (12) (1997) 1463–1472.
[68] M. Farajpour Mojdehi, S.F. Rafie, N. Abu-Zahra, O. Saghatchian, Z. Shams Ghamsari, F. Mahmoudi, H. Sayahi, S.M Hashemianzadeh, Exploring the mechanisms of diazinon adsorption onto alpha and beta cyclodextrins through molecular dynamics simulations: insights into environmentally friendly pesticide remediation, Results. Eng. 21 (2024) 102020.
[69] G. Gnanamoorthy, Z. Xiangyam, S. Magesh, Y. Guo, S. Munusamy, R. Kaviya, S. G. Jenifer, P. Chermakani, V.K. Yadav, J. Jin, Z. Lu, Advanced function of novel Ba2MnS3/rGO nanomaterials for enhanced photocatalytic, antibacterial, A549 cell line and molecular docking applications, Results. Eng. 28 (2025) 107018, https://doi.org/10.1016/j.rineng.2025.107018.
[70] S.K. Miryala, S. Basu, A. Naha, R. Debroy, S. Ramaiah, A. Anbarasu, et al., Identification of bioactive natural compounds as efficient inhibitors against Mycobacterium tuberculosis protein-targets: a molecular docking and molecular dynamics simulation study, J. Mol. Liq. (2021) 117340, https://doi.org/10.1016/j.molliq.2021.117340.
[71] J.A. Lemkul, Introductory tutorials for simulating protein dynamics with GROMACS, J. Phys. Chem. B 128 (39) (2024) 9418–9435, https://doi.org/10.1021/acs.jpcb.4c04901.
[72] F.B. Omage, J.A. Salim, I. Mazoni, I.H. Yano, J.E. Hernández González, J.G. Silva Júnior, et al., STINGAllo: a web server for high-throughput prediction of allosteric site-forming residues using internal protein nanoenvironment descriptors, Brief. Bioinform. 26 (4) (2025) bbaf424, https://doi.org/10.1093/bib/bbaf424.
[73] H.J. Choi, A.J. Lee, K.S. Kang, J.H. Song, B.T. Zhu, 4-Hydroxyestrone, an endogenous estrogen metabolite, can strongly protect neuronal cells against oxidative damage, Sci. Rep. 10 (1) (2020) 7283, https://doi.org/10.1038/s41598-020-62984-y.
[74] J.L. Wittliff, S.A. Andres, D.A. Kerr, Estrogens II: catechol, Estrogens, in: P. Wexler (Ed.), Encyclopedia of Toxicology, 2nd ed., Elsevier, 2005, pp. 248–251, https://doi.org/10.1016/B0-12-369400-0/10047-X.
[75] M. Kamal, R. Jockers, Bitopic ligands: all-in-one orthosteric and allosteric, F1000. Biol. Rep. 1 (2009) 77, https://doi.org/10.3410/B1-77.
[76] B.I. Gaiser, M. Danielsen, X. Xu, K.R. Jørgensen, P. Fronik, E. Märcher-Rørsted, et al., Bitopic ligands support the presence of a metastable binding site at the β_2 adrenergic receptor, J. Med. Chem. 67 (13) (2024 Jul 11) 1105311068, https://doi.org/10.1021/acs.jmedchem.4c00578. PMID: 38952152.
[77] J.H. Frisk, J.M. Vanoevelen, J. Bierau, G. Pejler, S. Eriksson, L. Wang, Biochemical characterizations of human TMPK mutations identified in patients with severe microcephaly: single amino acid substitutions impair dimerization and abolish their catalytic activity, ACS. Omega 6 (49) (2021 Dec 14) 33943–33952, https://doi.org/10.1021/acsomega.1c05288.
[78] R.A. Laskowski, M.B. Swindells, LigPlot+: multiple ligand–protein interaction diagrams for drug discovery, J. Chem. Inf. Model. 51 (10) (2011) 2778–2786, https://doi.org/10.1021/ci200227u.
[79] W. Kabsch, C. Sander, Dictionary of protein secondary structure: pattern recognition of hydrogen-bonded and geometrical features, Biopolymers 22 (12) (1983 Dec) 2577–2637, https://doi.org/10.1002/bip.360221211.
[80] R.T. McGibbon, K.A. Beauchamp, M.P. Harrigan, et al., MDTraj: a modern open library for the analysis of molecular dynamics trajectories, J. Chem. Theory. Comput. 11 (8) (2015) 4001–4014, https://doi.org/10.1021/acs.jctc.5b00255.
[81] E. Eyal, G. Lum, I. Bahar, The anisotropic network model web server at 2015 (ANM 2.0), Bioinformatics 31 (9) (2015) 1487–1489, https://doi.org/10.1093/bioinformatics/btu847.
[82] E. Akarova, N.V. Grishin, E.V. Koonin, The HicAB cassette, a putative novel, RNA-targeting toxin-antitoxin system in archaea and bacteria, Bioinformatics 22 (21) (2006) 2581–2584, https://doi.org/10.1093/bioinformatics/btl418.
[83] A. Naha, S. Banerjee, R. Debroy, et al., Network metrics, structural dynamics and density functional theory calculations identified a novel ursodeoxycholic acid

derivative against therapeutic target Parkin for Parkinson's disease, Comput. Struct. Biotechnol. J. 20 (2022) 4271–4287, https://doi.org/10.1016/j.csbj.2022.08.017. Published 2022 Aug 10.
[84] Z. Huang, L. Zhu, Y. Cao, G. Wu, X. Liu, Y. Chen, et al., Asd: a comprehensive database of allosteric proteins and modulators, Nucleic. Acids. Res. 39 (2011) D663–D669, https://doi.org/10.1093/nar/gkq1022.
[85] M. Bernetti, S. Bosio, V. Bresciani, F. Falchi, M. Masetti, Probing allosteric communication with combined molecular dynamics simulations and network analysis, Curr. Opin. Struct. Biol. 86 (2024) 102820, https://doi.org/10.1016/j.sbi.2024.102820.
[86] H. Wang, M.J. Hou, L. Liao, et al., Strong protection by 4-hydroxyestrone against erastin-induced ferroptotic cell death in estrogen receptor-negative human breast cancer cells: evidence for protein disulfide isomerase as a mechanistic target for protection, Biochemistry 63 (6) (2024) 984–999, https://doi.org/10.1021/acs.biochem.3c00261.
[87] M.S. El-Shoukrofy, A. Atta, S. Fahmy, D. Sriram, M.A. Mahran, I.M. Labouta, New tetrahydropyrimidine-1,2,3-triazole clubbed compounds: antitubercular activity and thymidine monophosphate kinase (TMPKmt) inhibition, Bioorg. Chem 131 (2023) 106312, https://doi.org/10.1016/j.bioorg.2022.106312.
[88] K.N. Venugopala, C. Tratrat, M. Pillay, et al., In silico design and synthesis of tetrahydropyrimidinones and tetrahydropyrimidinethiones as potential thymidylate kinase inhibitors exerting anti-TB activity against *Mycobacterium tuberculosis*, Drug Des. Dev. Ther. 14 (2020) 1027–1039, https://doi.org/10.2147/DDDT.S228381.
[89] M. Naik, A.K. Raichurkar, B. Bandodkar, et al., Structure guided lead generation for *Mycobacterium tuberculosis* thymidylate kinase (Mtb TMK): discovery of 3-cyanopyridone and 1,6-naphthyridin-2-one as potent inhibitors, J. Med. Chem. 58 (2) (2015) 753–766, https://doi.org/10.1021/jm5012947.
[90] V. Vanheusden, H. Munier-Lehmann, M. Froeyen, R. Busson, J. Rozenski, P. Herdewijn, S. Van Calenbergh, Discovery of bicyclic thymidine analogues as selective and high-affinity inhibitors of Mycobacterium tuberculosis thymidine monophosphate kinase, J. Med. Chem. 47 (25) (2004) 6187–6194, https://doi.org/10.1021/jm040847w.
[91] P. Xu, S. Huang, H. Zhang, et al., Structural insights into the lipid and ligand regulation of serotonin receptors, Nature 592 (7854) (2021) 469–473, https://doi.org/10.1038/s41586-021-03376-8.
[92] S. Zhang, J. Li, Q. Xu, W. Xia, Y. Tao, C. Shi, D. Li, S. Xiang, C. Liu, Conformational dynamics of an α-synuclein fibril upon receptor binding revealed by insensitive nuclei enhanced by polarization transfer-based solid-state nuclear magnetic resonance and cryo-electron microscopy, J. Am. Chem. Soc. 145 (8) (2023 Mar 1) 4473–4484, https://doi.org/10.1021/jacs.2c10854.
[93] J.R. Lane, P.M. Sexton, A. Christopoulos, Bridging the gap: bitopic ligands of G-protein-coupled receptors, Trends. Pharmacol. Sci. 34 (1) (2013) 59–66, https://doi.org/10.1016/j.tips.2012.10.003.
[94] T.R. Weikl, B. Hemmateenejad, How conformational changes can affect catalysis, inhibition and drug resistance of enzymes with induced-fit binding mechanism such as the HIV-1 protease, Biochim. Biophys. Acta 1834 (5) (2013) 867–873.
[95] M. Jayaraman, S.K. Rajendra, K. Ramadas, Structural insight into conformational dynamics of non-active site mutations in KasA: a Mycobacterium tuberculosis target protein, Gene 720 (2019), https://doi.org/10.1016/j.gene.2019.144082.
[96] A. Mishra, A.S. Mamidi, R.S. Rajmani, A. Ray, R. Roy, A. Surolia, An allosteric inhibitor of *Mycobacterium tuberculosis* ArgJ: implications to a novel combinatorial therapy, published correction appears in EMBO Mol Med. 2019 Oct;11(10):e11209. 10.15252/emmm.201911209.], EMBo Mol. Med. 10 (4) (2018) e8038, https://doi.org/10.15252/emmm.201708038.
[97] N. Hemavathy, S. Ranganathan, V. Umashankar, et al., Computational development of allosteric peptide inhibitors targeting LIM kinases as a novel therapeutic intervention, Cell Biochem. Biophys. (2025), https://doi.org/10.1007/s12013-025-01718-1.
[98] M. Amala, H. Nagarajan, M. Ahila, et al., Unveiling the intricacies of allosteric regulation in aspartate kinase from the Wolbachia endosymbiont of Brugia Malayi: mechanistic and therapeutic insights, Int. J. Biol. Macromol. 267 (Pt 1) (2024) 131326, https://doi.org/10.1016/j.ijbiomac.2024.131326.
[99] A.H. Newman, F.O. Battiti, A. Bonifazi, 2016 Philip S. portoghese medicinal chemistry lectureship: designing bivalent or bitopic molecules for G-protein coupled receptors. The whole is greater than the sum of its parts, J. Med. Chem. 63 (5) (2020) 1779–1797, https://doi.org/10.1021/acs.jmedchem.9b01105.
[100] H. Ma, B. Huang, Y. Zhang, Recent advances in multitarget-directed ligands targeting G-protein-coupled receptors, Drug Discov. Today 25 (9) (2020) 1682–1692, https://doi.org/10.1016/j.drudis.2020.07.004.